Journal of Magnetic Resonance 204 (2010) 314–326

Contents lists available at ScienceDirect

Journal of Magnetic Resonance

journal homepage: www.elsevier.com/locate/jmr

Dipolar-coupling-mediated total correlation spectroscopy in solid-state ^{13}C NMR: Selection of individual ^{13}C–^{13}C dipolar interactions

Justin Spano, Sungsool Wi *

Department of Chemistry, Virginia Tech, Blacksburg, VA 24061, USA

ARTICLE INFO

Article history:
Received 17 December 2009
Revised 10 March 2010
Available online 23 March 2010

Keywords:
^{13}C solid-state NMR
DTOCSY
Homonuclear dipolar recoupling
Uniformly labeled sample
Isolation/individualization of ^{13}C–^{13}C dipolar interaction

ABSTRACT

Herein is described a useful approach in solid-state NMR, for selecting homonuclear ^{13}C–^{13}C spin pairs in a multiple-^{13}C homonuclear dipolar coupled spin system. This method builds upon the zero-quantum (ZQ) dipolar recoupling method introduced by Levitt and coworkers (Marin-Montesinos et al., 2006 [30]) by extending the originally introduced one-dimensional (1D) experiment into a two-dimensional (2D) method with selective irradiation scheme, while moving the ^{13}C–^{13}C mixing scheme from the transverse to the longitudinal mode, together with a dramatic improvement in the proton decoupling efficiency. Selective spin-pair recoupling experiments incorporating Gaussian and cosine-modulated Gaussian pulses for inverting specific spins were performed, demonstrating the ability to detect informative, simplified/individualized, long-range ^{13}C–^{13}C homonuclear dipolar coupling interactions more accurately by removing less informative, stronger, short-range ^{13}C–^{13}C interactions from 2D correlation spectra. The capability of this new approach was demonstrated experimentally on uniformly ^{13}C–labeled Glutamine and a tripeptide sample, GAL.

Published by Elsevier Inc.

1. Introduction

Solid-state NMR (ssNMR) spectroscopy has evolved as a suitable technique for structure determination of a wide variety of sample systems including biomolecules, regardless of the sample's morphology [1–9]. Many techniques developed for structural investigation in ssNMR spectroscopy exploit heteronuclear or homonuclear dipolar couplings between spins to measure internuclear distances, while performing magic-angle-spinning (MAS) to obtain well resolved spectra [10–16]. These techniques developed in ssNMR spectroscopy provide distance information quantitatively when applied to a selectively labeled spin system that provides isolated dipolar interactions.

When applied on an extensively or uniformly labeled sample system, these techniques normally have limited accuracies for distance measurements. One difficulty that arises in performing such experiments is the dipolar truncation effect; the more informative long-range, weaker dipolar couplings are masked by the less informative short-range, stronger dipolar couplings [17–19]. Another type of complication arising from a uniformly labeled sample system is the relayed signal transfer; a signal transfer between two uncoupled nuclei via a third spin that is coupled to both spins [20]. While these problems may be alleviated by preparing selectively labeled samples, these preparations are time consuming and expensive compared to using uniformly labeled samples; not to mention, much more structural information can be gained from a uniformly labeled sample since many dipolar pairs, hence many geometrical constraints, are available.

Selective heteronuclear distance measurements were implemented in uniformly or extensively labeled samples in the platform of the rotational-echo double resonance (REDOR) technique [10] by incorporating frequency selective pulses to isolate a certain I–S spin interaction from a complicated I_mS_n spin system [21]. Moreover, multiple, simultaneous ^{13}C–^{15}N distance measurements that were free from any ^{13}C peak broadening effect due to ^{13}C–^{13}C homonuclear J-coupling interactions were accomplished in uniformly ^{13}C–^{15}N-labeled samples by employing the three-dimensional (3D) transferred echo double resonance (TEDOR) method, combined with a z-filtering or a selective π-pulse inversion scheme [22].

Various types of frequency selective techniques have also been developed to accurately measure homonuclear dipolar interactions by curing problems associated with extensively or uniformly labeled samples. The first generation of these techniques includes the rotational resonance (RR) [11,23] and rotational resonance in tilted frame (RRTR) [24,25] which reintroduce the homonuclear dipolar interaction when the chemical shift difference of two spins under consideration matches the MAS spinning frequency. A more elaborate extension of this approach, performed under constant-time mode combined with a selective irradiation scheme is the rotational resonance width (R^2W) technique [26–29], that

* Corresponding author. Fax: +1 540 231 3255.
E-mail address: sungsool@vt.edu (S. Wi).

1090-7807/$ - see front matter Published by Elsevier Inc.
doi:10.1016/j.jmr.2010.03.015

satisfactorily isolate longer range ^{13}C–^{13}C dipolar interactions in uniformly labeled sample systems by varying the spinning speed. These techniques work under moderate-to-slow spinning conditions with spin pairs of relatively big isotropic chemical shift differences. Recently, chemical shift assisted homonuclear dipolar recoupling methods that produce secularized zero-quantum (ZQ) dipolar Hamiltonians have been introduced. These include the truncated dipolar recoupling (TDR) [30], triple oscillating field technique (TOFU) [31], and zero-quantum shift evolution assisted selective homonuclear recoupling (ZQ-SEASHORE) [32] methods; these have been demonstrated to be useful for selectively measuring distances between homonuclear spin pairs in a weak coupling regime if the difference in chemical shifts between the nuclei in a certain spin pair is greater than the dipolar coupling between them. The TDR method utilizes a symmetry-based $C3_3^1$ technique [15,16,33,34] that reintroduces ZQ-homonuclear dipolar interactions, as well as the isotropic and anisotropic chemical shift interactions. The TOFU method uses triply oscillating rf fields that allow simultaneous recoupling of isotropic chemical shifts and ZQ-homonuclear dipolar interactions. The ZQ-SEASHORE method consist of alternating blocks of the radio-frequency-driven recoupling (RFDR) sequence [35,36] and free evolution time for chemical shift evolution. Here, the RFDR sequence reintroduces ZQ homonuclear interactions under a high MAS spinning speed (>30 kHz). Chemical shift interactions in the ZQ-SEASHORE, TOFU, and TDR methods truncate the flip-flop terms of ZQ-homonuclear dipolar interactions under a weak coupling regime, resulting in the secularized ZQ-homonuclear dipolar interactions that commute with one another. When combined with a selective irradiation scheme incorporating a Gaussian pulse for frequency selection under a constant-time mode, these methods are very promising for obtaining long-range distance information with minimal dipolar truncation effects. However, a secularized ZQ dipolar Hamiltonian requires a mixing mode along transverse magnetizations, which is less favorable than a mixing mode along longitudinal magnetizations, because of the unfavorable signal loss due to a T_2-relaxation, particularly when NMR signals possess short T_2-relaxation times or the proton decoupling power is not sufficient. A related technique to the ZQ-SEASHORE is the double-quantum shift evolution assisted selective homonuclear recoupling (DQ-SEASHORE) method [37]. This sequence includes alternating blocks of C7 [12], a symmetry-based DQ recoupling sequence, and chemical shift evolution period under a slow-to-moderate spinning condition. The frequency selectivity of DQ-SEASHORE is achieved by adjusting the lengths of the free precession periods.

One major challenge found from the original implementation of the TDR approach was that the desired ^{13}C–^{13}C homonuclear dipolar recouplings were hindered largely by ^{13}C–^{1}H heteronuclear dipolar couplings that were also reintroduced by the sequence [30]. Magnetizations in transverse mode are quickly attenuated during the mixing period when the mixing scheme is under residual ^{13}C–^{1}H dipolar couplings. This unfavorable signal attenuation effect along transverse mode by residual ^{13}C–^{1}H dipolar interaction persists even under a high power proton decoupling. This drawback found in the original approach led to Levitt and coworkers applying the sequence on a deuterated model compound. This manuscript describes an attempt to implement the $C3_3^1$ sequence as a longitudinal mixing block in the scheme of a standard two-dimensional (2D) NMR exchange experiment at the expense of direct secularization effect. However, this approach obtains the selection of ^{13}C–^{13}C dipolar interactions by incorporating a Gaussian or a cosine-modulated Gaussian pulse [38–40] into the center of the 2D mixing block to partially remove relayed signal transfers as well as dipolar truncation effects from the complicated spin network in the sample system. Furthermore, the removal of the devastating requirement of extreme proton decoupling power required for the original TDR approach makes this new approach a practical method within the normal decoupling condition for a protonated organic solid. In this scheme, the flip-flop terms of the ZQ-homonuclear dipolar Hamiltonian are utilized for in-phase signal transfers in the strong coupling regime when the isotropic and anisotropic chemical shift terms are refocused at the end of the basic $C3_3^1$ unit in the mixing sequence. So, the essential feature of this approach is to suppress the offset and anisotropic chemical shift terms, and it is achieved by π-pulses (composite π-pulses are used in our experiments) placed synchronously in the mixing pulse block. The major gain of this approach is the removal of the devastating requirement of the original TDR approach for an extreme proton decoupling power, which is impractical within the normal experimental condition for a protonated organic solid. Simplification or individualization of ^{13}C–^{13}C dipolar interactions are achieved by incorporating a Gaussian or a cosine-modulated Gaussian pulse [38–40] into the 2D mixing block to remove relayed signal transfers as well as dipolar truncation effects in some favorable conditions. Our approach is reminiscent of the TOCSY experiment [41], a solution state NMR spectroscopic technique that utilizes the flip-flop terms of *J*-coupling interactions in a strong coupling regime, because our approach utilizes the flip-flop terms of ZQ-homonuclear dipolar couplings for the mixing of longitudinal magnetizations in a strong coupling regime. Hence, we named our approach as the Dipolar-coupling-mediated TOtal Correlation SpectroscopY (DTOCSY) in solid-state NMR.

2. Materials and methods

Samples of ^{13}C-labeled Gly-[U-^{13}C]Ala-[U-^{13}C]Leu, [U-^{13}C]-Tyrosine, and [U-^{13}C]-Glutamine were used for testing the feasibility of solid-state ^{13}C DTOCSY spectroscopy. Amino acids, [U-^{13}C]-Tyrosine and [U-^{13}C]-Glutamine, were purchased from the Cambridge Isotope Laboratory (Andover, MA). The [U-^{13}C]-Tyrosine sample was dissolved in 1 M HCl solution and recrystallized by slow evaporation and the [U-^{13}C]-Glutamine sample was used without further treatment. ^{13}C-labeled tripeptide, Gly-[U-^{13}C]Ala-[U-^{13}C]Leu, was synthesized by Fmoc-based solid-state peptide synthesis at AnaSpec Inc. (San Jose, CA). The synthesized peptide was purified and identified by reverse-phase liquid chromatography and ion-spray ionization mass analyzer, respectively. Subsequently, the peptide was recrystallized by slow evaporation from an aqueous solution. About 20–40 mg of each sample was center-packed into a 4 mm MAS rotor with bottom and top spacers. The sample temperature was kept constant at 22 °C by using a Bruker BCU-X temperature control unit.

^{13}C DTOCSY NMR spectra were recorded on a Bruker Avance II 300 MHz spectrometer with ^{1}H and ^{13}C Larmor frequencies of 300.12 MHz and 75.48 MHz, respectively, using the pulse sequence depicted in Fig. 1A. The 2D experiment begins with ^{1}H magnetization, generated by a $\pi/2$ excitation pulse, being transferred to ^{13}C magnetizations by ramped cross-polarization (CP) for 1 ms. ^{13}C magnetizations are then allowed to evolve under the chemical shifts of ^{13}C's during the indirect time (t_1), after which they are converted into the longitudinal mode by a $\pi/2$ pulse for DTOCSY mixing. Following a $\pi/2$ read pulse after DTOCSY mixing, ^{13}C signals are acquired for the direct acquisition time (t_2). Fig. 1B illustrates the construction of the DTOCSY mixing sequence [30]. The basic superblock, spanning $12\tau_r$ in length, where τ_r is the rotor period, consists of four $C3_3^1$ units in combination with composite π-pulses, $(\pi/2_x - \pi_y - \pi/2_x)$, positioned at the $3\tau_r$ and $9\tau_r$ time points. The DTOCSY mixing time can be incremented by increasing m ($m = 1, 2, \ldots$) in order to observe longer range ^{13}C–^{13}C correlations. The experiment employed a MAS spinning speed, $\omega_r/2\pi = 6$ kHz,

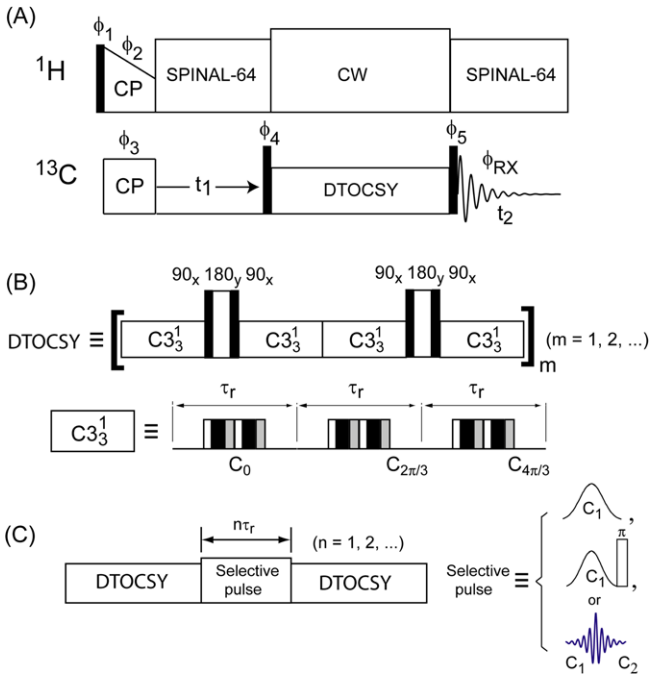

Fig. 1. (A) A standard 2D exchange spectroscopic pulse sequence used in this experiment incorporating the DTOCSY mixing block. Carbon magnetizations are created by CP from the proton channel and allowed for chemical shift evolution for t_1 before being converted into the longitudinal mode for DTOCSY mixing. Then, a 90° read pulse is required to convert signals into transverse mode for the direct signal acquisition for t_2. Closed rectangles represent $\pi/2$ pulses. Proton decoupling was achieved using SPINAL-64 [44] with 63 kHz power during the indirect (t_1) and acquisition periods (t_2), and 128 kHz CW decoupling power during DTOCSY mixing. Details of phase cycling steps are: $\phi_1 = y, -y$; $\phi_2 = x$; $\phi_3 = x, x, y, y, -x, -x, -y, -y$; $\phi_4 = y, y, -x, -x, -y, -y, x, x$; $\phi_5 = -y, -y, x, x, y, y, -x, -x, y, y, -x, -x, -y, -y, x, x$; $\phi_6 = x, -x, y, -y, -x, x, -y, y, -x, x, -y, y, x, -x, y, -y$. (B) Detailed schematic of the DTCOSY mixing sequence. This sequence is identical to the TDR sequence used by Levitt and coworkers except the composite π-pulses in the mixing block. Each DTOCSY block consists of a total of 4-$C3_3^1$ blocks, with composite π-pulses ($\pi/2_x$–π_y–$\pi/2_x$) placed at the $\tau_{mix}/4$ and $3\tau_{mix}/4$ positions of the DTOCSY sequence: the τ_{mix} of a single DTOCSY mixing unit takes 12 rotor periods ($12\tau_r$). At 6 kHz spinning, the length of a DTOCSY mixing block is therefore 2 ms. The DTOCSY mixing time increases by increasing the index m ($m = 1, 2, \ldots$). Each $C3_3^1$ block spans $3\tau_r$ and consists of three $\tau_r/4$–($\pi/2\phi$–2π $\phi\pi$–$3\pi/4\phi$–$\pi/2\phi\pi$–2π ϕ–$3\pi/4\phi$)–$\tau_r/4$ blocks; each block is phase-shifted by 120° with respect to the previous block. (C) A Gaussian, Gaussian plus a non-selective π or cosine-modulated Gaussian pulse placed in between DTOCSY mixing periods, spanning ideally an integer number of rotor periods, were employed to selectively irradiate certain spins in the ^{13}C spin network, which leads to spectral simplification. This composite pulse block takes $24\tau_r$ as a basic mixing time.

and 48 kHz (8 times the spinning speed) of DTOCSY mixing power to satisfy the condition for the symmetry-based sequence, $C3_3^1$. $C3_3^1$ consists of three phase-shifted $\tau_r/4 - (90^\circ\overline{360^\circ}270^\circ)_2 - \tau_r/4$ units for three rotor periods (Fig. 1B), and so a 360° pulse in this pulse block therefore has a length of $\tau_r/8$ [30]. Fig. 1C displays modified DTOCSY sequences for selective spin inversions formulated by inserting a Gaussian, a Gaussian plus a non-selective π, or cosine-modulated Gaussian pulse between two identical DTOCSY blocks. The Gaussian and cosine-modulated Gaussian pulses were generated by Bruker Topspin software with widths of 2–6τ_r. The offset frequency during the application of the selective pulse can be adjusted for optimal selective inversions. The ^{13}C and ^{1}H 90° pulse times were 5 μs and 3.5 μs, respectively, and spectra were acquired with 32 scans and a recycle delay of 3.5 s. The pulse power of composite ^{13}C π-pulses was 75 kHz. 2D ^{13}C–^{13}C correlation spectra were obtained with 1024 points in t_2 and 128 points in t_1, with 128 kHz of CW decoupling during DTOCSY mixing block and 63 kHz of SPINAL-64 [42] decoupling during the direct acquisition.

3. Theoretical

3.1. Background

As explained in the previous section, a symmetry-based dipolar recoupling method utilizing the $C3_3^1$ sequence, which was originally developed by Levitt and coworkers as the TDR technique for obtaining ^{13}C–^{13}C dipolar distances with a minimal dipolar truncation effect [30], can also be used in the standard two-dimensional (2D) correlation spectroscopy as an efficient mixing block applied upon longitudinal magnetizations (see Fig. 1). The $C3_3^1$ sequence gives the recoupling terms with space-spin quantum numbers of (l, m, λ, μ) = (2, ±2, 2, 0) and (2, ±1, 2, 0) in dipolar interactions, (l, m, λ, μ) = (2, ±2, 1, 0) and (2, ±1, 1, 0) of CSA, and (l, m, λ, μ) = (0, 0, 1, 0) of both J-coupling and isotropic chemical shift interactions [15,16,30,34]. Here, the rotational properties of the space and spin part of tensors in NMR interaction Hamiltonians are characterized by the rank l and components m ($m = -l, -l+1, \ldots, l-1, l$) and the rank λ and components μ ($\mu = -\lambda, -\lambda+1, \ldots, \lambda-1, \lambda$), respectively. A windowed double-post pulse element, $90^\circ\overline{360^\circ}270^\circ\overline{90^\circ}360^\circ\overline{270^\circ}$, for $\tau_r/4$–$3\tau_r/4$, combined with free evolution periods for 0–$\tau_r/4$ and $3\tau_r/4$–τ_r of each rotor period in a $C3_3^1$ unit, provides scaling factors of 0.138 and 0 for (2, ±1, 2, 0) and (2, ±2, 2, 0), respectively, of dipolar interaction; of 0.193 and 0 for (2, ±1, 1, 0) and (2, ±2, 1, 0), respectively, of CSA; and of 0.5 for (0, 0, 1, 0) of both isotropic chemical shift and J-coupling interactions [30]. The composite π-pulses placed after the first and third $C3_3^1$ blocks in the basic DTOCSY superblock refocuses both isotropic and anisotropic chemical shift interactions as well as the heteronuclear dipolar interaction terms at the end of basic $C3_3^1$ unit. Therefore, the remaining (2, ±1, 2, 0) term, which is the zero-order dipolar interaction, and (0, 0, 1, 0) term, which is the isotropic J-coupling interaction, will be effective at the end of the basic $C3_3^1$ sequence for in-phase signal transfers among magnetizations over the mixing periods. The flip-flop terms of the remaining ZQ dipolar Hamiltonian thus produce correlations between ^{13}C nuclei, mimicking the J-modulated TOCSY spectroscopy developed in solution state NMR. The influence of the isotropic J-coupling term in the DTOCSY mixing block is relatively insignificant as will be proved numerically in the next section.

3.2. In-phase DTOCSY signal transfer

An isolated homonuclear dipolar coupled spin pair, I–S ($I = S = ½$), is considered for understanding the basic characteristics of in-phase signal transfer of DTOCSY mixing. The average Hamiltonian, the (2, ±1, 2, 0) term of the zero-order dipolar interaction and the (0, 0, 1, 0) term of the isotropic J-coupling interaction, operative during the DTOCSY mixing is [30]:

$$\bar{\omega}_0 2I_zS_z + \bar{\omega}_\pm(I_xS_x + I_yS_y), \tag{1}$$

with $\bar{\omega}_0 = 2\pi(\nu_d + J/2)$ and $\bar{\omega}_\pm = 2\pi\nu_m = 2\pi(J - \nu_d)$, where ν_d and J are the strength of dipolar coupling and J-coupling interaction, respectively. Longitudinal magnetizations, $(I_z + S_z)$, under the influence of the average Hamiltonain during the DTOCSY mixing period are influenced only by the second term, $2\pi\nu_m(I_xS_x + I_yS_y)$, and propagate according to:

$$I_z \xrightarrow{2\pi\nu_m(I_xS_x+I_yS_y)\tau_m} I_z\cos^2(\pi\nu_m\tau_m) + S_z\sin^2(\pi\nu_m\tau_m) + (I_xS_y - I_yS_x)\sin(2\pi\nu_m\tau_m), \tag{2}$$

and

$$S_z \xrightarrow{2\pi\nu_m(I_xS_x+I_yS_y)\tau_m} I_z\sin^2(\pi\nu_m\tau_m) + S_z\cos^2(\pi\nu_m\tau_m) - (I_xS_y - I_yS_x)\sin(2\pi\nu_m\tau_m). \tag{3}$$

Eqs. (2) and (3) dictate that the sum, $I_z + S_z$, is constant and the difference, $I_z - S_z$, is given by:

$$(I_z - S_z) \xrightarrow{2\pi\nu_m(I_xS_x+I_yS_y)\tau_m} (I_z - S_z)\cos(2\pi\nu_m\tau_m) + 2(I_xS_y - I_yS_x)\sin(2\pi\nu_m\tau_m). \quad (4)$$

When $\tau_m = n/2\nu_m$ ($n = 1, 3, 5, \ldots$), I_z magnetization is completely transferred to S_z magnetization and vise versa. In crystalline powdered sample, the magnitude of ν_d is however orientationally dependent and therefore the signal transfer efficiency will show orientation dependency.

To test the efficiency of the in-phase signal transfer of our approach, brute force calculations were carried out using a home-built program written under Matlab programming environment on a dipolar coupled system taken from C′, C^α, and C^β carbons existing in an amino acid, explicitly considering all the relevant CSA, J, and dipolar interactions for DTOCSY mixing. Chemical shift parameters of C′, C^α, and C^β carbons, the dipolar coupling, and J-coupling parameters considered in the simulations are summarized in Table 1. The dipolar coupling between C′ and C^β is purposely not included in this simulation in order to clearly investigate the efficiency of the relayed signal transfer via $C' \rightarrow C^\alpha \rightarrow C^\beta$. The initial magnetization was given only to C′, and the signal transfer to C^α and C^β was monitored by increasing the mixing time of DTOCSY sequence. Fig. 2A and B shows thus obtained magnetization transfers, $C' \rightarrow C^\alpha$ and $C' \rightarrow C^\alpha \rightarrow C^\beta$, without (Fig. 2A) and with (Fig. 2B) considering J-coupling interactions between C′–C^α and C^α–C^β pairs. Both signal transfers occurred efficiently within the first point (<4 ms) and maintain efficiency within 20–30% for the $C' \rightarrow C^\alpha$ transfer and 10–12% for the $C' \rightarrow C^\alpha \rightarrow C^\beta$ transfer throughout the mixing times considered. As can be seen from these figures it is clear that the difference in the DTOCSY signal transfers with and without considering J-coupling interactions is not significant. The relayed fashion of signal transfer, $I_z \rightarrow S_z \rightarrow K_z$, would provide total correlation patterns among ^{13}C nuclei in the dipolar coupled network. This property together with the dipolar truncation effect would complicate quantitative peak interpretations. As will be explained in the next section, however, isolation of individual ^{13}C–^{13}C dipolar interactions in 2D DTOCSY spectra can be achieved in some favorable cases by incorporating selective inversion of magnetizations utilizing a soft pulse, such as a Gaussian or cosine-modulated Gaussian pulse.

Table 1
Chemical shift parameters incorporated for simulations in Fig. 2.

	δ_{iso} (ppm)	δ_{CSA} (ppm)	η	ν_d (C′–C^α)	ν_d (C^α–C^β)
C′	120	81	0.91	2.18 kHz	2.22 kHz
C^α	0	35	035	J (C′–C^α)	J (C^α–C^β)
C^β	−15	30	0.3	55 Hz	35 Hz

Chemical shift tensor parameters are defined as $\delta_{CSA} = \delta_{zz} - \delta_{iso}$ and $\eta = (\delta_{xx} - \delta_{yy})/\delta_{CSA}$, where $|\delta_{zz} - \delta_{iso}| \geqslant |\delta_{xx} - \delta_{iso}| \geqslant |\delta_{yy} - \delta_{iso}|$ and $\delta_{iso} = (\delta_{xx} + \delta_{yy} + \delta_{zz})/3$.

Similar to the J-coupling mediated proton TOCSY spectroscopy developed in solution state NMR [41], the offset difference, the relative peak separation between the coupled nuclei, influences the efficiency of the DTOCSY mixing significantly in general. However, as can be seen in the previous simulations (Fig. 2) and the following experimental spectra (Figs. 7–9), the offset tolerance of the DTOCSY signal transfer was evidenced in the usual chemical shift ranges of C′ and C^α and C^β at the spinning speeds of 6–8 kHz. The signal transfer between C′ and C^α was very efficient (20–30%) although the isotropic chemical shift difference between C′ and C^α (120 ppm) and the magnitude of CSA of C′ (δ_{CSA} = 81 ppm, η = 0.91) were very large.

Optimal in-phase ^{13}C–^{13}C correlations, observed by utilizing the flip-flop terms of the ZQ dipolar Hamiltonian that are reintroduced by $C3_3^1$ sequence, have demonstrated offset-dependent dipolar recoupling conditions that reminisce the rotational resonance condition. The offset dependence on the $I_z \rightarrow S_z$ transfer efficiency was investigated by varying the offset frequencies of both nuclei, I_z and S_z, from −150 ppm to 150 ppm in the simulations as shown in Fig. 3. The $I_z \rightarrow S_z$ signal transfer is efficient at spots on the 2D map satisfying $|\delta_1 - \delta_2| = n\nu_r$ (n = 0, 1, and 2), where δ is the offset frequency and ν_r is the spinning speed, with about 40–50 ppm widths per each spot along both offset dimensions. The origin of this phenomenon is not clear, but the isotropic chemical shift difference between dipolar coupled spins obviously takes a role that when it matches to the spinning frequency the dipolar coupling strength between these spins reintroduces more effectively, as in the case of the rotational resonance mechanism [11]. For instance, two adjacent favorable regions along each offset dimension are separated from each other by the MAS spinning frequency as can be identified in Fig. 3B, which is about 80 ppm (ω_r = 6 kHz; ω_0 = 75 MHz). Regions having efficient $I_z \rightarrow S_z$ signal transfer in

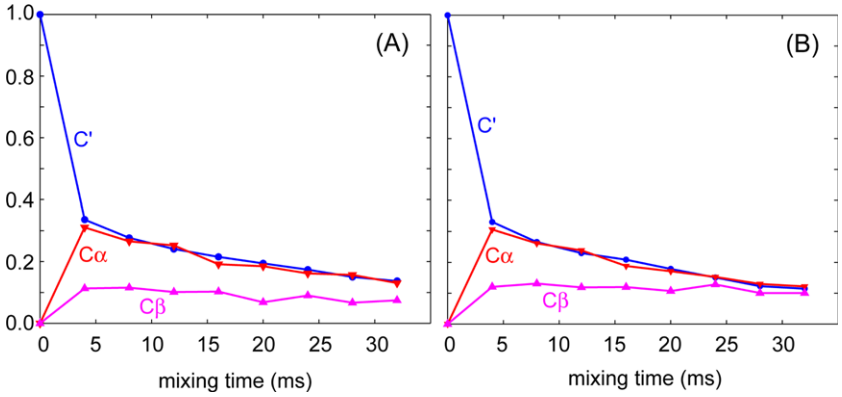

Fig. 2. DTOCSY simulations on a three-spin system, C′–C^α–C^β, in the standard geometry of an amino acid, demonstrating the efficiencies of $C' \rightarrow C^\alpha$ and $C' \rightarrow C^\alpha \rightarrow C^\beta$ signal transfers via dipolar couplings. The J-coupling influence is negligible as the simulation data without (A) and with (B) the J-coupling influences do not show any significant differences. Dipolar coupling strengths are calculated based on the known C′–C^α (2.18 kHz) and C^α–C^β (2.22 kHz) distances, but the C′–C^β coupling was omitted in the simulation to calculate the relayed signal transfer, $C' \rightarrow C^\alpha \rightarrow C^\beta$ explicitly isotropic and anisotropic chemical shifts of typical C′, C^α, and C^β carbons as well as the J-coupling parameters of C′–C^α (55 Hz) and C^α–C^β (35 Hz) bonds were considered, while taking the isotropic chemical shift position of C^α as the on-resonance point. Initially, only the longitudinal magnetization of C′ was assigned before applying DTOCSY mixing. Directly bonded C′–C^α transfer reaches the maximum efficiency at the first point of the mixing time and maintains 20–30% of efficiency throughout the mixing time, while gradually decreasing its efficiency as the mixing time increases. The relayed signal transfer also reached its maximum efficiency at the first point and maintains about 10% relative efficiency throughout the mixing time.

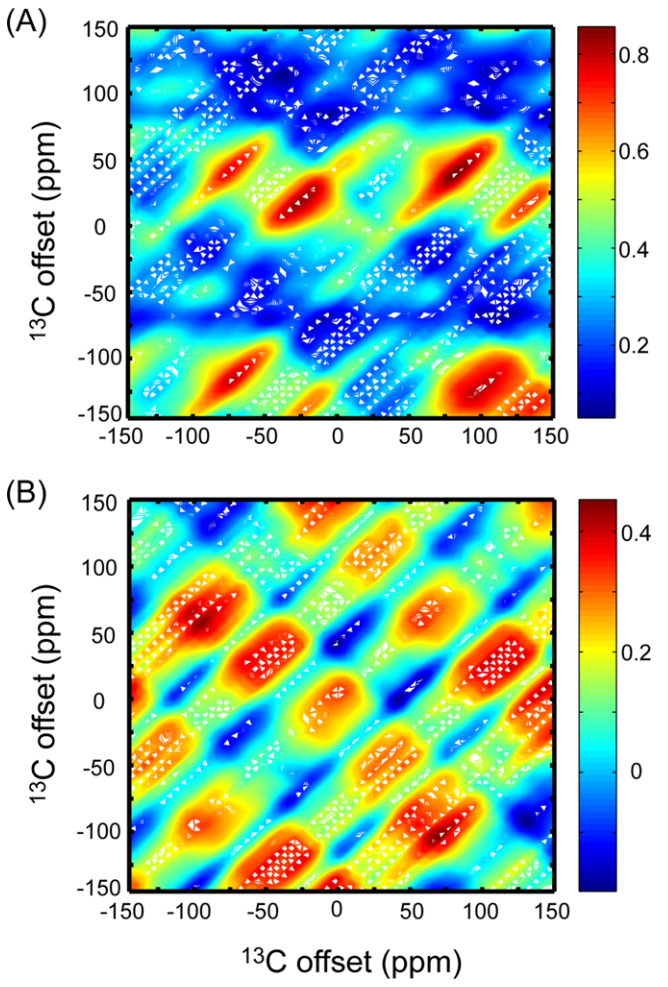

Fig. 3. Simulations showing the offset dependencies of the $I_z \rightarrow S_z$ DTOCSY signal transfer. The $I_z \rightarrow S_z$ DTOCSY signal transfer was calculated by changing the offset frequencies of I and S spins from −150 ppm to 150 ppm (ω_0 = 75 MHz), considering arbitrarily a dipolar coupling strength of 1.2 kHz, and defining the CSA of I and S nuclei as 81 ppm (η = 0.91) and 30 ppm (η = 0.30), respectively. We provided only the I_z magnetization initially and monitored the $I_z \rightarrow S_z$ transfer (B) as well as the remaining I_z magnetization (A) by changing the offsets of both nuclei. Contour levels incorporated in each map indicate relative signal intensities of the remained I_z (A) and the transferred S_z magnetizations (B) that are normalized by the initial input intensity of the I_z magnetization. In (B), many favorable $I_z \rightarrow S_z$ transfer conditions that are formed roughly at the frequencies satisfying $|\delta_1 - \delta_2| = n\nu_r$ (n = 0, 1, and 2), where δ is the offset frequency and ν_r is the spinning frequency, are evidenced on the two-dimensional map, with a width of ~50 ppm along both offset domains per a single favorable spot.

Fig. 3B correspond to the regions of low I_z signal in Fig. 3A in most cases. However, some regions with low I_z signal intensity do not possess efficient $I_z \rightarrow S_z$ transfer; these regions would produce efficient $I_z \rightarrow 2(I_xS_y - I_yS_x)$ transfers, where the $2(I_xS_y - I_yS_x)$ term corresponds to the zero-quantum coherence.

3.3. Simplification of correlations and selection of individual dipolar interactions

For simplifying a 2D ^{13}C–^{13}C DTOCSY spectrum and/or isolating individual dipolar interactions, we incorporated a Gaussian, a Gaussian with a non-selective 180° pulse, or a cosine-modulated Gaussian pulse in the DTOCSY sequence as outlined in Fig. 1C. A selective inversion pulse block is concatenating two identical ZQ-recoupling pulse blocks of the same period of mixing time along both sides, so that the action of the first ZQ-recoupling sequence is refocused by the second sequence when the selective inversion pulse between them inverts a spin in a dipolar coupled pair. Thus, any ^{13}C–^{13}C dipolar couplings that involve only a single inverted spin will be removed from the 2D correlations in the spectra at the end of the composite DTOCSY block. When a spin is irradiated using a selective inversion pulse, the selected spin possesses a negative diagonal-peak and takes suppressed cross-peaks with any non-selected spins in the network. If both spins of a dipolar pair are inverted by a selective pulse, then the dipolar interaction is retained after the overall mixing block. The cross-peaks between two selected spins are retained with negative intensities. A dipolar coupling interaction between two non-selected spins should maintain untouched state, therefore, provides both positive diagonal- and cross-peak intensities in a 2D spectrum.

These predictions can easily be verified by considering the evolution of magnetizations under the influence of the composite DTOCSY mixing block, incorporating a selective pulse. For an I–S spin pair, when a Gaussian pulse that is placed in the middle of the two identical ZQ-recoupling mixing periods invert only the I-spin, the signal produced by the whole DTOCSY mixing block will be:

$$I_z \xrightarrow{2\pi\nu_m\tau_m(I_xS_x+I_yS_y)} \xrightarrow{180^\circ_x(I)} \xrightarrow{2\pi\nu_m\tau_m(I_xS_x+I_yS_y)} -I_z\cos(2\pi\nu_m\tau_m) + 2I_yS_x\sin(2\pi\nu_m\tau_m). \quad (5)$$

Therefore, the action of the pulse block results in an inverted I_z spin and $2I_yS_x$ term, a half the original ZQ-coherence terms produced without the selective π-pulse (Eqs. (2) and (3)), while producing no in-phase signal transfer to S spin. Likewise, the non-irradiated S spin evolves under the I-spin irradiation according to:

$$S_z \xrightarrow{2\pi\nu_m\tau_m(I_xS_x+I_yS_y)} \xrightarrow{180^\circ_x(I)} \xrightarrow{2\pi\nu_m\tau_m(I_xS_x+I_yS_y)} S_z\cos(2\pi\nu_m\tau_m) - 2I_xS_y \times \sin(2\pi\nu_m\tau_m). \quad (6)$$

The pulse block still does not produce the in-phase $S_z \rightarrow I_z$ signal transfer, and keeps the original sign of S_z spin as expected because it was not irradiated by the inversion pulse. Furthermore, combining Eqs. (5) and (6), the DTOCY pulse block with I-spin irradiation results in the zero-quantum coherence term, $2(I_yS_x - I_xS_y)$, which is still half of the ZQ-coherence terms obtained without selective π-pulse, that can be removed at the time points satisfying $\tau_m = n/2\nu_m$ (n = 1, 2, …), where $\nu_m = J - \nu_d$, and J and ν_d are ^{13}C–^{13}C J-coupling and dipolar coupling constants, respectively. At these time points of the mixing period, the I–S homonuclear dipolar coupling is null. Thus, an I–S dipolar coupling can be removed completely from the spin network at these time points in the mixing time when either I- or S-spin is inverted.

Now, if both I and S spins are inverted simultaneously by, for instance, a cosine-modulated Gaussian pulse, the $I_z \rightarrow S_z$ signal transfer is retained with both spins inverted:

$$I_z \xrightarrow{2\pi\nu_m\tau_m(I_xS_x+I_yS_y)} \xrightarrow{180^\circ_x(I,S)} \xrightarrow{2\pi\nu_m\tau_m(I_xS_x+I_yS_y)} -I_z\cos^2(2\pi\nu_m\tau_m) - S_z \times \sin^2(2\pi\nu_m\tau_m) + (I_yS_x - I_xS_y)\sin(4\pi\nu_m\tau_m). \quad (7)$$

Similarly, the $S_z \rightarrow I_z$ transfer is provided as:

$$S_z \xrightarrow{2\pi\nu_m\tau_m(I_xS_x+I_yS_y)} \xrightarrow{180^\circ_x(I,S)} \xrightarrow{2\pi\nu_m\tau_m(I_xS_x+I_yS_y)} -S_z\cos^2(2\pi\nu_m\tau_m) - I_z \times \sin^2(2\pi\nu_m\tau_m) + (I_xS_y - I_yS_x)\sin(4\pi\nu_m\tau_m). \quad (8)$$

The sum of Eqs. (7) and (8) is just $-(I_z + S_z)$, therefore, when both I and S spins are irradiated, the spectral correlation between I and S spin can be isolated from the rest of dipolar correlations involving other spins in a 2D spectrum. Potential relayed signal transfers from non-radiated spins to I or S spin can be effectively blocked in this mode. However, the removal of dipolar interactions with non-irra-

diation spins is marginal due to the presence of ZQ-coherence terms formed with non-irradiated spins, for instance, $2(I_yK_x - I_xK_y)$ or $2(S_yK_x - S_xK_y)$ terms, where K is a non-irradiated spin, except those time points specified by $\tau_m(IK) = n/2\nu_m(IK)$ and $\tau_m(SK) = n/2\nu_m(SK)$, $(n = 1, 2, \ldots)$. A complete isolation of an I–S spin pair from a three-spin system, I–S–K, would be feasible at certain time points. However, when multiple spin pairs are involved, it would be impractical to remove many ZQ-coherence terms formed between non-irradiated spins and I or S spins simultaneously. Thus, a simultaneous I and S spin irradiation does provide a way to remove signal transfers via relayed fashions as well as dipolar truncation effects partially. Therefore, this irradiation mode would be useful for isolating a specific ^{13}C–^{13}C interaction more precisely from the crowded interactions in the spin network originating from an extensively/uniformly labeled protein/peptide sample. Practically, effective irradiation on both I and S spins would depend on the frequency selection efficiency of selective inversion pulses, the inversion profiles of selected frequency ranges, and the length of the DTOCSY mixing sequence used in the experiment. A selective soft pulse or a magnitude-modulated selective soft pulse scheme that provides narrow, but uniform inversion profiles in the chosen spectral windows would be necessary for the effectiveness of selecting a particular dipolar interaction for distance measurement.

Fig. 4 shows numerically simulated signal transfers among nuclear spins in a hypothetical, model 3-^{13}C-spin system under the DTOCSY mixing, incorporating a selective inversion pulse as introduced herein, with corresponding spin network diagrams drawn. The Larmor frequency and the MAS spinning speed used are 75 MHz and 8 kHz, respectively, the magnitudes of isotropic and anisotropic chemical shift parameters are shown in the inset table of the figure, and the strength of dipolar couplings involved are designated in the spin network diagram in the figure. Unless specified explicitly, our simulations assumed 100 kHz of the pulse power for the $90_x180_y90_x$ composite pulses and coincident dipolar/dipolar and dipolar/CSA tensor orientations. In Fig. 4A is shown a simulation in which the homonuclear dipolar coupling between all three ^{13}C spin pairs in the network are considered without a selective inversion pulse. Beginning with longitudinal magnetization of C_1 being fed into the mixing block, the C_1 magnetization can then be transferred to C_2 and C_3 through homonuclear dipolar couplings, reducing the relative intensity of C_1 and increasing the relative intensity of C_2 and C_3, as expected. Initially there is a much faster buildup of for C_2 than for C_3 due to the stronger C_1–C_2 homonuclear dipolar coupling interaction. After reaching a maximum value, there is a constant intensity region or even a small decrease in relative C_2 intensity at a long mixing time. Fig. 4B and C demonstrate the effect of a selective soft pulse applied on C_2 and C_3, respectively, in the 3-^{13}C-spin system, with the corresponding spin network diagrams shown adjacent to the relative intensity plots. Fig. 4B shows the effect of the selective irradiation on C_2. It can be seen that the $C_1 \rightarrow C_2$ transfer is virtually zero, and there is only significant magnetization transfer for $C_1 \rightarrow C_3$. Due to the weak C_1–C_3 homonuclear dipolar coupling, and absence of $C_1 \rightarrow C_2 \rightarrow C_3$ contribution, magnetization buildup for C_3 takes slightly longer as compared to Fig. 4A. When the selective inversion pulse inverts C_3 (Fig. 4C), there is almost no noticeable magnetization buildup

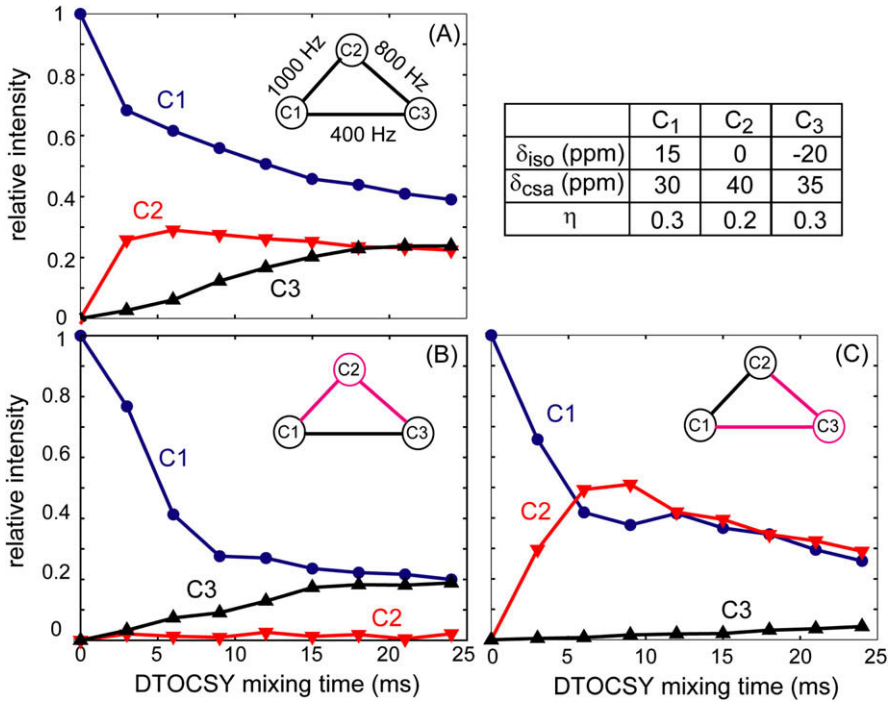

	C_1	C_2	C_3
δ_{iso} (ppm)	15	0	-20
δ_{csa} (ppm)	30	40	35
η	0.3	0.2	0.3

Fig. 4. Simulations showing the selective signal transfers incorporating a Gaussian pulse in the DTOCSY block, demonstrated for the different ^{13}C sites in a hypothetical model 3-^{13}C-spin system. Isotropic and anisotropic chemical shift tensors of three spin sites are shown in the inset table. The C_1–C_2, C_1–C_3, and C_2–C_3 homonuclear dipolar coupling strengths are 1 kHz, 0.2 kHz, and 0.8 kHz, respectively, as indicated in the inset diagram in the figure. Relative orientations between the dipolar and CSA tensors are ignored for simplicity. The spins in the system are designated as C_1 (blue circles with blue solid line), C_2 (red triangles with red solid line), and C_3 (black inverted triangles with black solid line). Simulations showing the effect of the absence (A) or presence of a single Gaussian pulse irradiated at C_2 (B) and C_3 (C) are demonstrated. In all cases longitudinal magnetization of C_1 is provided as the initial source of magnetization for the system; this magnetization can then be transferred to other spins in the system via homonuclear dipolar coupling. The intensities of the magnetization for the different spins over time is relative to the original C_1 magnetization at time = 0. Selectively irradiated spins are designated in the spin network diagrams as pink circles with pink arrows focused on them, with the bonds from those spins also highlighted in pink to indicate which spin pairs would have suppressed homonuclear dipolar coupling interactions. A dipolar interaction which involves a single inverted spin is suppressed as can be identified in the simulations. Unless specified explicitly, the pulse power considered for the $90_x180_y90_x$ composite π-pulse (see Fig. 1) is 100 kHz in all our simulations. (For interpretation of the references to color in this figure legend, the reader is referred to the web version of this article.)

for the irradiated spin, C_3, but a quick relative intensity buildup for C_2. The C_2 signal experiences a quicker buildup with C_3 irradiation since it is not losing its magnetization to C_3.

To examine the efficacy of a spin pair selection of the DTOCSY sequence combined with an amplitude-modulated Gaussian pulse introduced herein, the spin system was extended to look at a hypothetical, model 4-^{13}C-spin system (Fig. 5); the theoretical relative intensity plots for different cases are shown with their corresponding spin network diagrams adjacent. The magnitudes of isotropic and anisotropic chemical shift parameters considered in the simulations are summarized in the inset table of Fig. 5. The Larmor frequency and the MAS spinning speed used are 75 MHz and 6 kHz, respectively, and the strength of dipolar couplings involved are designated in the spin network diagram. In Fig. 5A is shown the case where all of the homonuclear dipolar coupling interactions between the spins in the network are considered without a selective pulse. The relative intensity of C_2 and C_3, which each has homonuclear dipolar coupling strength of 1 kHz with C_1, has faster buildup than C_4, which only has 700 Hz of dipolar coupling with C_1. C_2 and C_3 possess identical dipolar coupling strengths with C_1, however, C_3 has a slower build-up curve than C_2 because of the difference in offset frequencies; the relative offset of C_3 from C_1 is -35 ppm, whereas the offset of C_2 from C_1 is 15 ppm. Fig. 5B exhibits the case where a cosine-modulated Gaussian pulse simultaneously irradiates both C_1 and C_2. As predicted by Eq. (7), the relative intensity plot demonstrates the retention of $C_1 \rightarrow C_2$ magnetization transfer and suppression of transfers to C_3 and C_4, as shown by the overall low intensities of C_3 and C_4 signals. This is to be expected since inverting the magnetizations of both C_1 and C_2 will retain the homonuclear dipolar coupling between them, while greatly suppressing the dipolar coupling interactions with C_3 and C_4.Simulations shown in Fig. 6 examine the finite pulse effect of the composite π-pulse, $90_x180_y90_x$, in the sequence (Fig. 1), and the non-coincident dipolar/dipolar and dipolar/CSA tensor orientations. Here, a three-spin system considered in Fig. 4 was incorporated again with non-coincident dipolar/CSA (Fig. 6A) and dipolar/dipolar (Fig. 6B) tensor orientations (see the figure caption for the details of relative tensor orientations). Based on our numerical simulations, both non-coincident dipolar/CSA (Fig. 6A) and dipolar/dipolar (Fig. 6B) interactions decrease the efficiencies of internuclear signal transfers, as can be identified by comparing both Fig. 6A and B to Fig. 4A, which corresponds to the case of assuming coincident dipolar/dipolar and dipolar/CSA tensor orientations. This may imply that if a ZQ-dipolar recoupling technique, such as RFDR or $R6_6^2$ [33], that is capable of suppressing chemical shift interactions is incorporated in the mixing scheme, the interference between dipolar and CSA tensors can be eliminated. Demonstrated in Fig. 6C is a finite rf pulse effect that results in less efficient magnetization transfers when an insufficient pulse power (50 kHz) is used for the composite π-pulses in the sequence. However, as demonstrated in Fig. 6D, when a single π-pulse version is used in the sequence, again the overall magnetization transfer is much less efficient than that of the case involving composite π-pulse version, even with a 100 kHz of rf pulse power. Therefore, it is crucial to incorporate composite π-pulses in the sequence of $C3_3^1$ to achieve better refocusing of chemical shifts, particularly when non-negligible offset differences or rf pulse inhomogeneities are involved in the experiments. In Fig. 6C and D, we assumed coincident dipolar/dipolar and dipolar/CSA orientations for simplicity.

4. Experimental results

One of the objectives in developing the pulse sequence introduced herein is to address the devastating proton decoupling problem of the original TDR approach by applying the sequence along the longitudinal mode of magnetizations as a mixing block of a standard 2D homonuclear correlation scheme. We have tested continuous wave (CW), TPPM [43], SPINAL-64 [44], and COMARO-2 [45], at various ^{1}H decoupling strengths during DTOCSY mixing

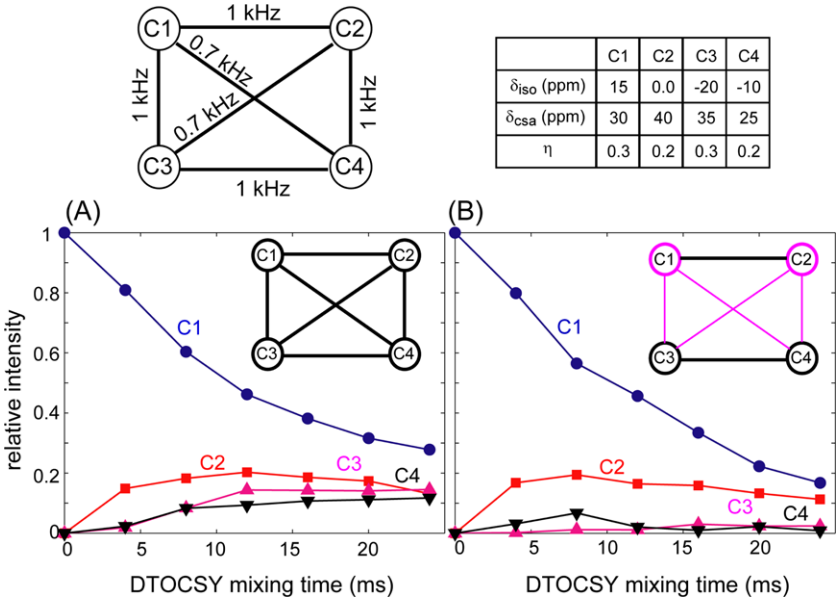

	C1	C2	C3	C4
δ_{iso} (ppm)	15	0.0	-20	-10
δ_{csa} (ppm)	30	40	35	25
η	0.3	0.2	0.3	0.2

Fig. 5. Simulations shown demonstrate a retention of dipolar coupling when both spins are irradiated. A hypothetical model, a 4-^{13}C-spin system, was considered under DTOCSY mixing over time in the absence (A) or presence (B) of a selective, cosine-modulated Gaussian pulse placed in between TDR mixing blocks. The spins in the system are designated as C_1 (blue circles with blue solid line), C_2 (red squares with red solid line), C_3 (pink triangles with solid pink line), and C_4 (black inverted triangles with black solid line). As in Fig. 4, longitudinal magnetization of C_1 is provided as the initial source of magnetization for the 4-^{13}C-spin system. The dipolar coupling strengths of spin pairs in the 4-^{13}C-spin systems are shown adjacent to the plots, with the C_1–C_2 = C_1–C_3 = C_2–C_4 = C_3–C_4 (1 kHz) and C_1–C_4 = C_2–C_3 (0.7 kHz). The magnitudes of isotropic and anisotropic chemical shift interactions are specified in the inset table. Relative orientations between the dipolar and CSA tensors are ignored for simplicity. As predicted by Eq. (6), selectively irradiated spins in a dipolar pair, which are indicated in the same manner as in Fig. 4, provide the retention of the signal transfer, with inverted intensities (B). (For interpretation of the references to color in this figure legend, the reader is referred to the web version of this article.)

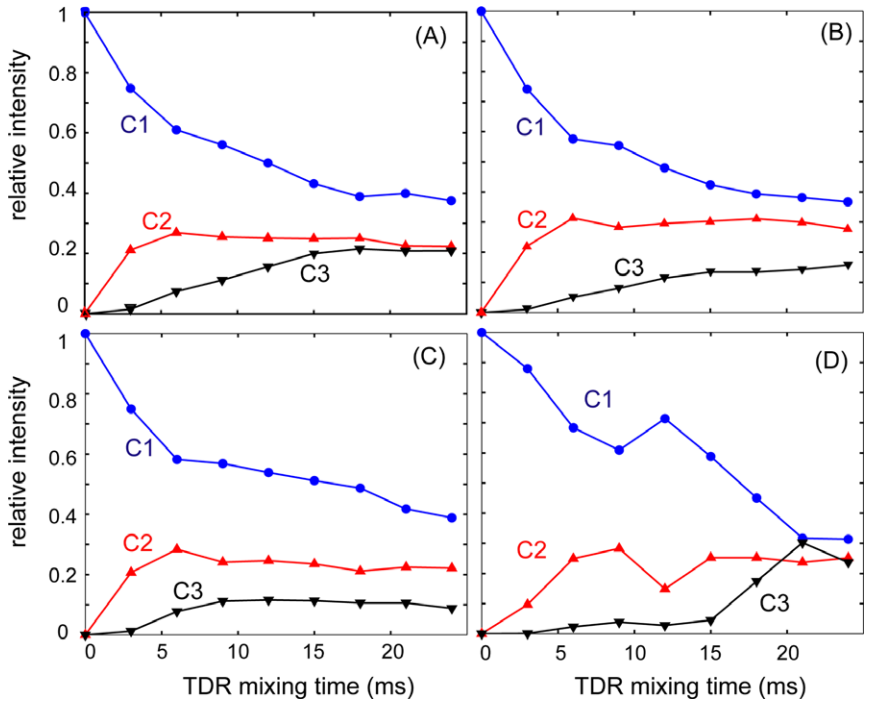

Fig. 6. Simulations showing finite pulse effect and the effect of non-coincident relative tensor orientations (dipolar/CSA, or dipolar/dipolar vectors) demonstrated on the three ^{13}C sites considered in Fig. 4. The intensities of magnetization for the different spins over time is relative to the original C_1 magnetization provided at time = 0. (A) Represents a case with non-coincident dipolar and CSA tensors, while maintaining the orientations of three dipolar vectors in parallel: $\mathrm{CSA}(C_1)\overset{(30^\circ,20^\circ,0^\circ)}{\rightarrow}D(C_1-C_2)$; $\mathrm{CSA}(C_2)\overset{(20^\circ,20^\circ,0^\circ)}{\rightarrow}D(C_1-C_2)$; $\mathrm{CSA}(C_3)\overset{(10^\circ,30^\circ,0^\circ)}{\rightarrow}D(C_1-C_2)$. (B) Corresponds to a case with non-parallel dipolar vectors, while maintaining coincident dipolar and CSA tensors: $D(C_1-C_3)\overset{(0^\circ,30^\circ,0^\circ)}{\rightarrow}D(C_1-C_2)$; $D(C_2-C_3)\overset{(0^\circ,40^\circ,0^\circ)}{\rightarrow}D(C_1-C_2)$. (C) Demonstrates a finite pulse effect with 50 kHz pulse power for the $90_x180_y90_x$ composite π-pulses in the sequence. D shows an ill efficiency of signal transfers among spin sites when a single π-pulse version is incorporated in the sequence instead of the original composite pulse version, even with 100 kHz rf pulse power. All coincident dipolar and CSA tensor orientations are considered in (C) and (D).

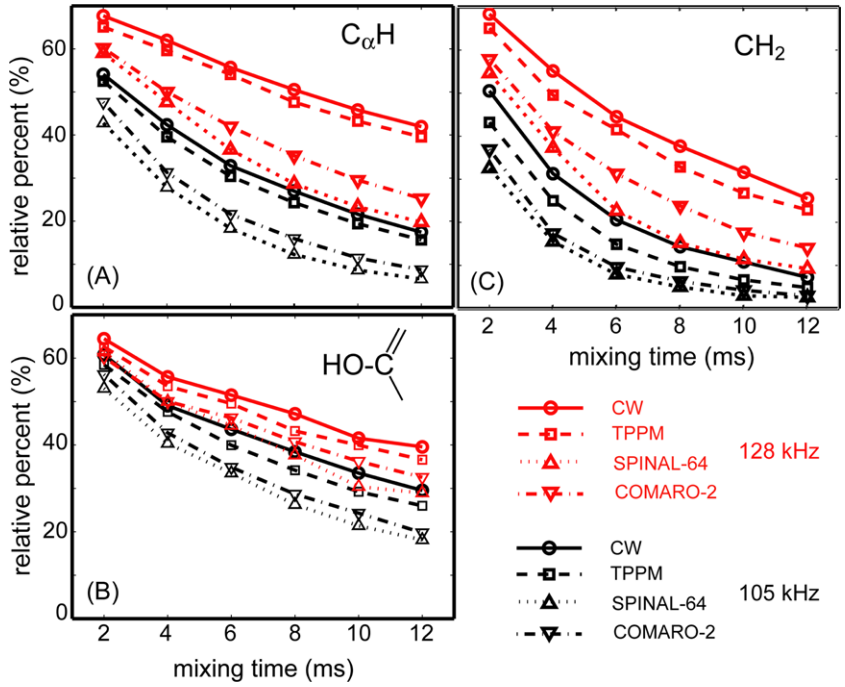

Fig. 7. Experimental ^{13}C signal intensity curves demonstrating the efficiency of different types of proton decoupling schemes with two different decoupling frequencies, applied during the DTOCSY mixing period: CW (circles with a solid line), TPPM (squares with a dashed line), [49] SPINAL-64 (triangles with a dotted line), [44] and COMARO-2 (inverted triangles with a dashed-dotted line) [45]. Decoupling efficiencies of these methods were compared by inspecting experimental data obtained on the C^α (A), C' (B), and C^β (C) of the [U-^{13}C, ^{15}N]-Tyrosine·HCl, at decoupling rf field strengths of 105 kHz (black) and 128 kHz (red). The relative intensities displayed were found by comparing experiments in which DTOCSY mixing was performed to experiments where DTOCSY mixing was excluded. In both cases, the CW mode is proved as the best decoupling mode among the specified methods when combined with DTOCSY sequence. The decoupling efficiency with a CW mode at 128 kHz ($\nu_1(^{13}C)$ = 48 kHz) was acceptable for all three types of carbons throughout the mixing time up to 12 ms. (For interpretation of the references to color in this figure legend, the reader is referred to the web version of this article.)

period for performing ^{13}C–^{1}H heteronuclear dipolar decoupling; the spinning speed and thus the power of ^{13}C channel during DTOCSY block were 6 kHz and 48 kHz, respectively. As a demonstration of our efforts, in Fig. 7 is shown the signal intensities of various ^{13}C sites in [U-^{13}C, ^{15}N]-Tyrosine·HCl, such as C′, C^{α}, and C^{β}, displaying how they vary as a function of DTOCSY mixing time under decoupling strengths of 128 kHz (red) and 105 kHz (black). To examine the efficiency for each decoupling technique, the intensity ratio of two experiments was calculated: (1) an experiment in which DTOCSY mixing is applied and (2) one where DTOCSY mixing is not used while maintaining the same delay time used for the DTOCSY sequence. In this approach, the proton decoupling problem is bypassed as can be seen in Fig. 7. The application of a proton decoupling strength, $\nu_1(^1H) \geqslant 2$–$2.3\nu_1$ (^{13}C), a typical decoupling power requirement for obtaining dipolar or CSA recoupling along the carbon channel [46,47], was sufficient. As expected, by looking at Fig. 7A–C, it can be noted that C′ with no attached protons is least sensitive to the heteronuclear decoupling techniques, followed by C^{α} with one attached proton, and CH_2 with two attached protons is most sensitive. For the most part, taking into account the plots for all three sites, there is a consistent trend among the peak intensity curves that there is greater efficiency at 128 kHz decoupling, and in terms of the different methods, CW was the most efficient, follow by TPPM, COMARO-2, and SPINAL-64.Fig. 8 shows experimentally obtained ^{13}C–^{13}C homonuclear correlation spectra of a three amino acid peptide, Gly-[U-^{13}C, ^{15}N]Ala-[U-^{13}C, ^{15}N]Leu, measured at $\nu_r = 6$ kHz and ν_1 $(C3_3^1) = 48$ kHz, with 128 kHz of proton decoupling power and mixing time $\tau_{mix} = 2$–20 ms ($l_2 = 1, 2, \ldots, 10$). For instance, Fig. 8A demonstrates spectral correlations measured at $l_2 = 5$ ($\tau_{mix} = 10$ ms) for the appropriate regions that show diagonal and cross-peaks. Diagonal peaks are visible for the different ^{13}C sites in Gly–Ala–Leu, along with many cross-peaks for different ^{13}C–^{13}C correlations. An important feature to discern from the 2D spectrum is that long-range homonuclear ^{13}C–^{13}C dipolar coupling interactions such as C_L^{δ}—C_L' (4-bond distance) are observable in the presence of short-range (i.e. 1-bond distance) interactions such as C_L^{α}—C_L' even without applying a selective pulse at, for instance, C_L^{alpha}. Other clearly distinguishable long-range ^{13}C–^{13}C dipolar cross-peaks include C_A^{β}—C_A', C_L^{β}—C_L', C_L^{α}—C_L^{γ}, C_L^{α}—C_L^{δ}, C_L'—C_L^{γ}, and even C_A'—C_L^{δ}. Some other notable features are a broad diagonal peak attributed to a combination of the resonances of one of the side chain methyl groups, C_L^{δ}, and the side chain methine group, C_L^{γ}, of leucine, and a doublet-like feature assigned to the sidechain resonances of the C_A^{β} of alanine and the other sidechain terminal C_L^{γ} of leucine. The X-ray determined structure of tripeptide Gly-Ala-Leu is included in the Fig. 8A for the reference of the ^{13}C–^{13}C dipolar pairs indicated, with an indication of sites that are ^{13}C labeled.Fig. 8B emphasizes the spectral region of

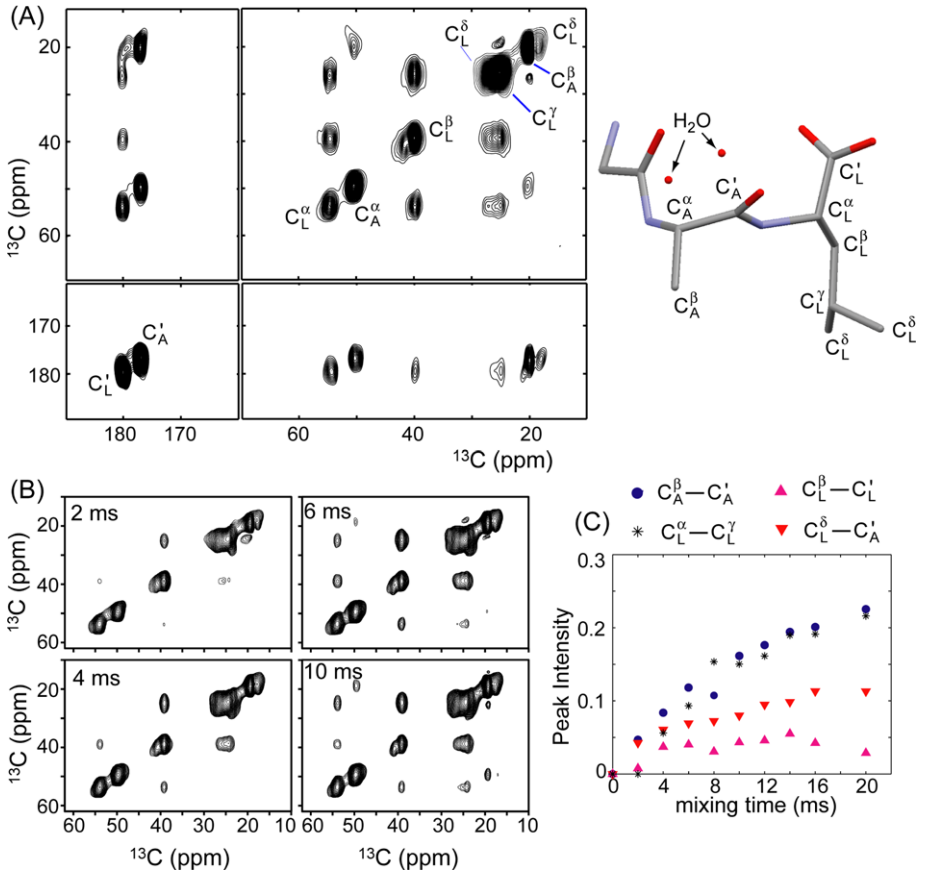

Fig. 8. 2D ^{13}C DTOCSY spectra of the 20% Gly-[U-^{13}C, ^{15}N]Ala-[U-^{13}C, ^{15}N]Leu in natural abundance Gly-Ala-Leu sample. (A) A full view of the 2D ^{13}C–^{13}C correlation spectrum, emphasizing only the frequency regions containing peaks, obtained with the pulse sequence shown in Fig. 1A with $\tau_{mix} = 20$ ms ($l_2 = 10$), without a selective pulse. The labeled carbon sites in the sample are designated along the diagonal peaks. Various types of short- and long-range ^{13}C–^{13}C cross correlations are evidenced in the spectra. (B) Changes in the cross-peak intensities in the 2D map, emphasizing the 0–60 ppm aliphatic region in both dimensions, as the DTOCSY mixing time increases from 2 ms to 10 ms. Cross peak correlations identified include: short-range interactions, such as C_A^{α}—C_A', C_L^{α}—C_L', C_A^{α}—C_A^{β}, C_L^{α}—C_L^{β}, and C_L^{β}—C_L^{γ}; long-range interactions, such as C_A^{β}—C_A', C_L^{β}—C_L', C_L^{γ}—C_L', C_L^{α}—C_L^{γ}, and C_L^{δ}—C_L'. (C) Dipolar build-up curves for various ^{13}C–^{13}C correlations, showing how the relative intensity varies as a function of DTOCSY mixing time: C_A^{β}—C_L^{δ}—$C_L'C_A'$ (blue closed circles), $C_L^{\alpha} - C_L^{\gamma}$ (black asterisk), $C_L^{\beta} - C_L'$ (pink triangles), and (inverted red triangles). Relative intensity was found by taking the ratio of the total cross-peak intensity to the total diagonal peak intensity for each spin pair. The X-ray determined structure of the Gly-Ala-Leu sample is shown as an inset with the designation of carbon sites. (For interpretation of the references to color in this figure legend, the reader is referred to the web version of this article.)

10–60 ppm for both direct and indirect spectral domains with mixing times τ_{mix} = 2 (l_2 = 1), 6 (l_2 = 3), 10 (l_2 = 5), and 14 ms (l_2 = 7). Cross-peak intensities, particularly for the longer range ^{13}C–^{13}C coupling pairs, clearly increase as the mixing time increases. Fig. 8C illustrates the dipolar ^{13}C–^{13}C build-up curves of C^{β}_{A}—C'_{A} (blue circle), C^{α}_{L}—C^{γ}_{L} (star), C^{β}_{L}—C'_{L} (inverted red triangle), and C'_{A}—C^{δ}_{L} (purple triangle) obtained by increasing the DTOCSY mixing time. Cross-peak intensities are divided by diagonal peak intensities for signal normalization. Among these build-up curves, the relative intensity buildup was highest for C^{β}_{A}—C'_{A} and C^{α}_{L}—C^{γ}_{L}, followed by C'_{A}—C^{δ}_{L}, and lowest for C^{β}_{L}—C'_{L}. Magnetization transfers are influenced by the magnitude of dipolar interactions, the presence of intervening dipolar interactions, the spinning frequency, isotropic offsets, and anisotropic chemical shifts including the relative tensor orientations between dipolar and chemical shift tensors. In Figs. 9 and 10 are shown the results of experiments involving selective inversion pulses for simplifying correlation patterns or selecting individual couplings. By inserting a selective Gaussian or a cosine-modulated Gaussian in the middle of DTOCSY mixing block, it was possible to selectively attenuate or maintain specific dipolar coupling interactions as predicted by Eqs. (5)–(8) and demonstrated in Figs. 4 and 5. Fig. 9 shows the resulting 2D ^{13}C–^{13}C correlation spectrum from an experiment with a selective Gaussian inversion pulse irradiated at the C^{α} carbons in Gly-[U-^{13}C, ^{15}N]Ala-[U-^{13}C, ^{15}N]Leu peptide. As compared to Fig. 8A, indeed any dipolar pairs involving C^{α} carbons are not appreciable in Fig. 9, while retaining correlations between spin pairs not involving C^{α}. Some resulting spectral features are the negative diagonal-peak intensities of the inverted C^{α} sites (colored in red) and the suppressed cross-peak intensities of any correlations involving C^{α}s. It may facilitate to measure the weaker dipolar interaction more accurately by removing the stronger one if the strong and weaker couplings share a spin. For instance, a selective inversion of a C^{α} carbon will improve the accuracy of measurements of the C'—C^{β} interaction and other long-range intra-residue ^{13}C–^{13}C interactions involving the C' carbon.Fig. 10 shows the 2D ^{13}C–^{13}C correlation spectrum of a model compound U-^{13}C Glutamine obtained from an experiment with simultaneous selective irradiations at two frequency regions (Fig. 10C), along with reference spectra obtained from the standard approach without a selective pulse (Fig. 10A) and from an experiment with a selective Gaussian pulse (Fig. 10B). A cosine-modulated Gaussian pulse was used to simultaneously irradiate both 160–180 ppm and 20–35 ppm regions to invert carbonyl carbons and all the aliphatic carbons except the C^{α}. To achieve a single site inversion we used a Gaussian pulse at the C^{α} carbon as before (Fig. 9). Again, the inverted diagonal peaks obtained with the Gaussian and the cosine-modulated Gaussian pulses are represented with red contour lines. As explained in the theoretical section, simultaneous inversions at two frequency regions provide a way to better isolate a ^{13}C–^{13}C dipolar coupling from a spin network because it retains a dipolar interaction if both nuclei in the pair are inverted simultaneously, while removing any homonuclear correlations in a 2D spectrum if only one spin in a pair is inverted. However, the removal of dipolar interactions with non-irradiated spins is marginal because only the half of the ZQ-coherence terms with non-irradiated spins is removed by simultaneous I and S spin irradiations. Upon comparing Fig. 10A and B, negative, but clear cross-peak intensity for C^{γ}—C^{δ} and $(C^{\beta}$—$C^{\delta}) + (C^{\beta}$—$C')$ are evidenced in Fig. 10C, but cross-peaks involving the C^{α} carbon are suppressed. Also shown in Fig. 10 are dipolar build-up curves for the cross-peak intensities for the C^{γ}—C^{δ} and the unresolved $(C^{\beta}$—$C^{\delta}) + (C^{\beta}$—$C')$ correlations measured without selective pulse (Fig. 10A), with a selective Gaussian pulse (Fig. 10B), and with a selective cosine-modulated Gaussian pulse (Fig. 10C) over the mixing times of 0–26 ms. Interestingly, two different cases with selective inversions (Fig. 10B and C) show dipolar build-up curves with higher efficiencies, demonstrating that these selective dipolar recoupling methods, particularly the scheme with a cosine-modulated Gaussian pulse, can minimize dipolar truncation effects and signal loss due to the relayed signal

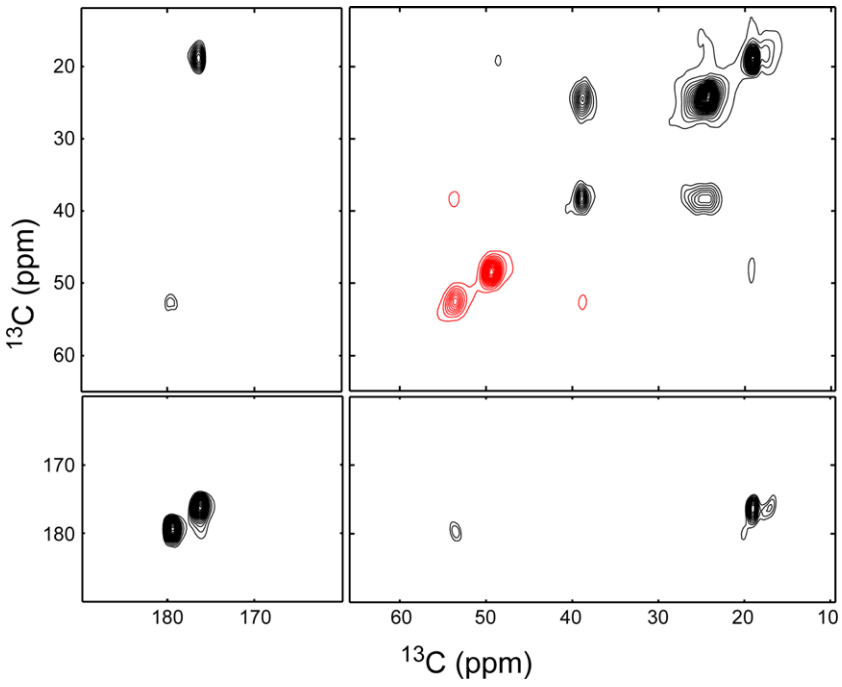

Fig. 9. 2D ^{13}C–^{13}C correlation spectrum obtained from a DTOCSY experiment incorporating a selective Gaussian pulse set to irradiate C^{α}_{L} and C^{α}_{A}; red contour lines are used to indicate the inverted C^{α} diagonal peaks. By comparing this spectrum with Fig. 7A, the spectral simplification resulting from using a selective Gaussian pulse can be noticed; any correlations involving the C^{α}_{L} and C^{α}_{A} spins are suppressed. (For interpretation of the references to color in this figure legend, the reader is referred to the web version of this article.)

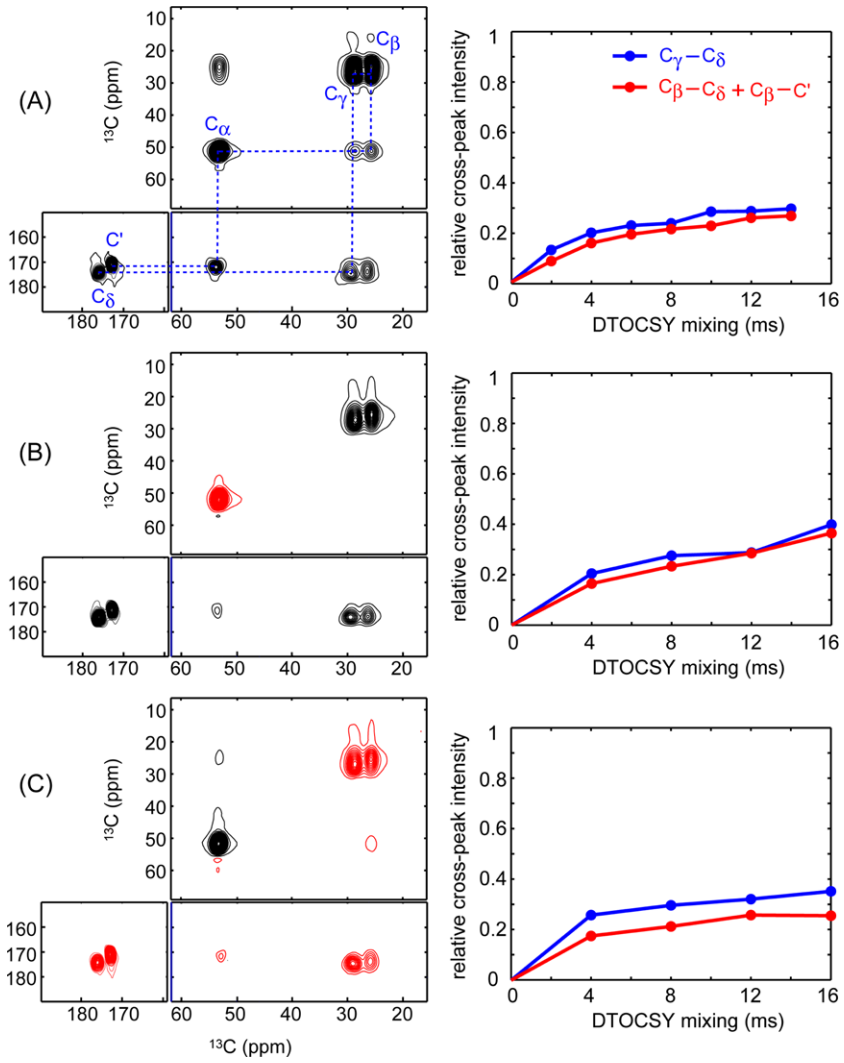

Fig. 10. 2D ^{13}C–^{13}C correlation spectra of a model compound U-^{13}C Glutamine obtained from a DTOCSY experiment in which a selective cosine-modulated Gaussian pulse is used to simultaneously irradiate two frequency regions (C′, C^β, C^γ, and Cδ) in a spectrum (C); the 2D ^{13}C–^{13}C correlation spectra from experiments without any selective pulse (A) and with a single Gaussian pulse irradiated at C^α (B) are shown as references. By comparing Fig. 9C with the reference spectra, (A) and (B), an individualization of dipolar pairs involving carbon sites that are simultaneously irradiated by a cosine-modulated Gaussian pulse can be noticed; red contour lines are used to indicate inverted diagonal and cross-peaks. Dipolar build-up curves for the cross-peaks, C^γ–Cδ and C^β–Cδ + C^β–C′ (C), are shown for each at the three scenarios. Notice that a selective pulse is sandwiched by two DTOCSY mixing blocks with an identical mixing time in the selective mixing scheme. In this particular case, (B) and (10) are identical in nature and, indeed, the build-up curves from both modes are very similar to each other. (For interpretation of the references to color in this figure legend, the reader is referred to the web version of this article.)

transfers. Hence, DTOCSY method would be an advanced tool for measuring specific spin pairs more accurately in a complicated dipolar network in homonuclear 2D correlation spectroscopy.

5. Discussion

Herein we have demonstrated a new approach in 2D ssNMR to correlate ^{13}C–^{13}C dipolar couplings in the longitudinal mode, combining a symmetry-based technique introduced by Levitt and coworkers with a selective irradiation scheme, that is useful for selecting/simplifying ^{13}C–^{13}C homonuclear dipolar coupling interactions from complicated dipolar networks. This method would enable simplifications of 2D correlation patterns and extraction of certain structurally important ^{13}C–^{13}C interactions more clearly by eliminating the appearance of other ^{13}C–^{13}C homonuclear dipolar couplings in a two-dimensional (2D) correlation spectrum. It also improves the accuracy of distance measurements of weak dipolar coupling interactions by partially eliminating terms that are responsible to the relayed signal transfers and dipolar truncation effects through the use of selective irradiation schemes. According to our numerical simulations, efficient DTOCSY signal transfers occur when the offset difference of two nuclei involved in a dipolar pair corresponds to zero, one, and two times the MAS spinning frequency used, reminiscing a rotational resonance condition. The width of each frequency window that shows a favorable signal transfer is about 3–4 kHz (40–50 ppm). The exact mechanism of the occurrence of this rotational resonance type effect is not clear, but we hypothesize that the chemical shift interactions reintroduced by the $C3_3^1$ sequence interfere with the spinning frequency. This hypothesis can be justified by the fact that a similar effect was not visible in our simulations when a pure ZQ-recoupling technique, such as RFDR sequence, is used in the mixing block.As we have tested various heteronuclear dipolar decoupling schemes at different rf strengths, it was found that if the proton decoupling power is at least 2.3 times the ^{13}C channel pulse power, which is in turn 8 times the MAS spinning speed, the CW decoupling mode provided acceptable decoupling efficiency for DTOCSY

mixing applied along longitudinal magnetizations. For instance, we have used 128 kHz of CW proton decoupling power, 48 kHz of DTOCSY mixing power, and 6 kHz of MAS speed in our experiments (Figs. 7–10). Using a ^{13}C, ^{15}N-labeled Gly-Ala-Leu sample in an experiment with non-selective recoupling of ^{13}C–^{13}C homonuclear dipolar coupling interactions, it was able to simultaneously observe multiple long-range ^{13}C–^{13}C correlations (i.e. C'_A—C^{δ}_L) in the presence of short-range interactions (i.e. C^{α}_L—C'_L) (Fig. 8).The adverse effect of insufficient ^{13}C–^{1}H heteronuclear dipolar decoupling during $C3^1_3$ mixing, originally reported with the introduction of TDR, was removed by switching the mixing scheme from the transverse mode of magnetization to the longitudinal mode. Contrary to the methods that produce secularized ZQ-homonuclear dipolar terms, such as TDR and ZQ-SEASHORE, the DTOCSY method utilizes the flip-flop terms of ZQ-homonuclear dipolar terms, which makes two dipolar coupling interactions that share a common spin not commute with each other. However, when a selective irradiation pulse is incorporated in the mixing scheme, it provides an alternative route of selecting individual ^{13}C–^{13}C dipolar interactions. Particularly, as shown in Fig. 10C, it provides a potential route for extracting a single ^{13}C–^{13}C dipolar interaction with improved accuracy from a network of multiple ^{13}C–^{13}C dipolar interactions by simultaneously irradiating both spins involved in a coupling. This ability might provide much control in studying homonuclear dipolar coupling interactions to obtain more accurate distance measurements from a complicated dipolar network. The longitudinal mixing mode also provides an advantage over the transverse mixing mode in that it can incorporate a longer mixing time even when NMR signals possess short T_2-relaxation times. For reference, the $C3^1_3$ -based DTOCSY scheme can be compared to one incorporating a conventional ZQ-dipolar recoupling method. For instance, the RFDR technique under a slow-to-moderate spinning condition [35] possesses a compatibility with a selective irradiation scheme, thus, can be used as a recoupling block in DTOCSY mixing scheme. This simpler approach would possess an advantage over the $C3^1_3$ sequence in that it reintroduces only ZQ-dipolar interactions with a shorter time in the basic mixing unit. Based on our numerical simulations (data not shown), the RFDR-based mixing scheme, for instance, has demonstrated an additional advantage over the $C3^1_3$ -based scheme in that it is capable of isolating a very weak ^{13}C–^{13}C interaction (ca. 300 Hz) from a stronger one (ca. 2.2 kHz) when these two couplings share a common spin in a dipolar coupled network. However, the RFDR-based scheme possesses a limited capability over the $C3^1_3$-based method when coupled spin sites are separated by small chemical shift differences. In general, the optimal recoupling regions and the range of dipolar coupling strengths that can be isolated are strongly dependent on the type of recoupling method incorporated in the DTOCSY mixing scheme. A popular ssNMR technique, proton-driven spin diffusion (PDSD) [48], which provides correlations of long-range ^{13}C–^{13}C couplings even when the chemical shift differences between the coupled spins are significant, is not compatible with a selective irradiation pulse in the DTOCSY scheme as introduced herein, and therefore, can not be used for simplifying or isolating a specific interaction from 2D correlations.

The ZQ-SEASHORE method that individualizes homonuclear dipolar couplings based on the secularization of the ZQ dipolar Hamiltonian is not feasible as a mixing scheme for longitudinal magnetizations because the secularized, effective dipolar Hamiltonian produced through this technique commutes with longitudinal magnetizations. Moreover, the ZQ-SEASHORE method is applicable only at high spinning speed (>30 kHz), while the DTOCSY method is advantageous if a slow-to-moderate spinning speed is inevitable in an experiment. Based on the results of this study, it is expected that the DTOCSY scheme, with appropriate ZQ-recoupling method and selective irradiation scheme, may provide an advantageous route with improved sensitivity and accuracy in studying selective spin pairs from uniformly labeled samples for elucidating structures of biological molecules.

The shape and efficiency of the selective pulse decides the selectivity in the frequencies as well as the inversion profile of the selected frequency ranges. A Gaussian or a cosine-modulated Gaussian pulse provides a relatively limited region of uniform inversion over the specified frequency ranges, particularly when the inversion window is small. Future efforts with the DTOCSY technique should focus on developing a selective pulse scheme that provides a narrow, uniform inversion profile over the specified spectral window, as this should improve the effectiveness of DTOCSY for individualizing spin pair interactions from complicated dipolar networks.Currently, we are exploring the feasibility of various types of symmetry-based ZQ homonuclear recoupling methods Levitt and coworkers developed, such as $SR4^1_4$ and $SR6^2_6$ [33], as a basic DTOCSY mixing block to improve the efficiency at isolating weak ^{13}C–^{13}C dipolar interactions in the presence of strong one-bond ^{13}C–^{13}C dipolar interactions.

Acknowledgments

This work is supported by Jeffress Memorial Trust Fund (J-815) and by the NSF (CHE-0541764).

References

[1] S. Opella, NMR and membrane proteins, J. Nat. Struct. Biol. 4 (1997) 845.
[2] R.G. Griffin, Dipolar recoupling in MAS spectra of biological solids, Nat. Struct. Mol. Biol. 5 (1998) 508.
[3] H.J.M. De Groot, Solid-state NMR spectroscopy applied to membrane proteins, Curr. Opin. Struct. Biol. 10 (2000) 593.
[4] R. Tycko, Biomolecular solid state NMR: advances in structural methodology and applications to peptide and protein fibrils, Annu. Rev. Phys. Chem. 52 (2001) 575.
[5] F. Castellani, B. van Rossum, A. Diehl, M. Schubert, K. Rehbein, H. Oschkinat, Structure of a protein determined by solid-state magic-angle-spinning NMR spectroscopy, Nature 420 (2002) 98.
[6] R. Tycko, Progress towards a molecular-level structural understanding of amyloid fibrils, Curr. Opin. Struct. Biol. 14 (2004) 96.
[7] A.E. McDermott, Structural and dynamic studies of proteins by solid-state NMR spectroscopy: rapid movement forward, Curr. Opin. Struct. Biol. 14 (2004) 554.
[8] M. Baldus, Molecular interactions investigated by multi-dimensional solid-state NMR, Curr. Opin. Struct. Biol. 16 (2006) 618.
[9] A. Lange, K. Giller, S. Hornig, M.F. Martin-Eauclaire, O. Pongs, S. Becker, M. Baldus, Toxin-induced conformational changes in a potassium channel revealed by solid-state NMR, Nature 440 (2006) 959.
[10] T. Gullion, J. Schaefer, Rotational-echo double-resonance NMR, J. Magn. Reson. 81 (1989) 196.
[11] D.P. Raleigh, M.H. Levitt, R.G. Griffin, Rotational resonance in solid state NMR, Chem. Phys. Lett. 146 (1988) 71.
[12] Y.K. Lee, N.D. Kurur, M. Helmle, O.G. Johannessen, N.C. Nielsen, M.H. Levitt, Efficient dipolar recoupling in the NMR of rotating solids. A sevenfold symmetric radiofrequency pulse sequence, Chem. Phys. Lett. 242 (1995) 304.
[13] S. Dusold, A. Sebald, Dipolar Recoupling Under Magic-Angle Spinning Conditions, Annual Reports on NMR Spectroscopy, Academic Press, 2000.
[14] R. Tycko, G. Dabbagh, Measurement of nuclear magnetic dipole–dipole couplings in magic angle spinning NMR, Chem. Phys. Lett. 173 (1990) 461.
[15] M. Carravetta, M. Ed, X. Zhao, A. Brinkmann, M.H. Levitt, Symmetry principles for the design of radiofrequency pulse sequences in the nuclear magnetic resonance of rotating solids, Chem. Phys. Lett. 321 (2000) 205.
[16] A. Brinkmann, M.H. Levitt, Symmetry principles in the nuclear magnetic resonance of spinning solids: heteronuclear recoupling by generalized Hartmann–Hahn sequences, J. Chem. Phys. 115 (2001) 357.
[17] M. Hohwy, C.M. Rienstra, C.P. Jaroniec, R.G. Griffin, Fivefold symmetric homonuclear dipolar recoupling in rotating solids: application to double quantum spectroscopy, J. Chem. Phys. 110 (1999) 7983.
[18] S. Kiihne, M.A. Mehta, J.A. Stringer, D.M. Gregory, J.C. Shiels, G.P. Drobny, Distance measurements by dipolar recoupling two-dimensional solid-state NMR, J. Phys. Chem. A 102 (1998) 2274.
[19] P. Hodgkinson, L. Emsley, The accuracy of distance measurements in solid-state NMR, J. Magn. Reson. 139 (1999) 46.
[20] J. Schmedt auf der Günne, Effective dipolar couplings determined by dipolar dephasing of double-quantum coherences, J. Magn. Reson. 180 (2006) 186.
[21] C.P. Jaroniec, B.A. Tounge, J. Herzfeld, R.G. Griffin, Frequency selective heteronuclear dipolar recoupling in rotating solids: accurate ^{13}C–^{15}N distance measurements in uniformly 13C,15N-labeled peptides, J. Am. Chem. Soc. 123 (2001) 3507.

[22] C.P. Jaroniec, C. Filip, R.G. Griffin, 3D TEDOR NMR experiments for the simultaneous measurement of multiple carbon–nitrogen distances in uniformly 13C,15N-labeled solids, J. Am. Chem. Soc. 124 (2002) 10728.
[23] A.T. Petkova, R. Tycko, Rotational resonance in uniformly ^{13}C-labeled solids: effects on high-resolution magic-angle spinning NMR spectra and applications in structural studies of biomolecular systems, J. Magn. Reson. 168 (2004) 137.
[24] K. Takegoshi, K. Nomura, T. Terao, Rotational resonance in the tilted rotating frame, Chem. Phys. Lett. 232 (1995) 424.
[25] K. Nomura, K. Takegoshi, T. Terao, K. Uchida, M. Kainosho, Determination of the complete structure of a uniformly labeled molecule by rotational resonance solid-state NMR in the tilted rotating frame, J. Am. Chem. Soc. 121 (1999) 4064.
[26] P.R. Costa, B. Sun, R.G. Griffin, Rotational resonance NMR: separation of dipolar coupling and zero quantum relaxation, J. Magn. Reson. 164 (2003) 92.
[27] R. Ramachandran, V. Ladizhansky, V.S. Bajaj, R.G. Griffin, ^{13}C–^{13}C rotational resonance width distance measurements in uniformly ^{13}C-labeled peptides, J. Am. Chem. Soc. 125 (2003) 15623.
[28] P.C.A. van der Wel, M.T. Eddy, R. Ramachandran, R.G. Griffin, Targeted C-13–C-13 distance measurements in a microcrystalline protein via J-decoupled rotational resonance width measurements, ChemPhysChem 10 (2009) 1656.
[29] X. Peng, D. Libich, R. Janik, G. Harauz, V. Ladizhansky, Dipolar chemical shift correlation spectroscopy for homonuclear carbon distance measurements in proteins in the solid state: application to structure determination and refinement, J. Am. Chem. Soc. 130 (2008) 359.
[30] I. Marin-Montesinos, G. Mollica, M. Carravetta, A. Gansmuller, G. Pileio, M. Bechmann, A. Sebald, M.H. Levitt, Truncated dipolar recoupling in solid-state nuclear magnetic resonance, Chem. Phys. Lett. 432 (2006) 572.
[31] N. Khaneja, N.C. Nielsen, Triple oscillating field technique for accurate distance measurements by solid-state NMR, J. Chem. Phys. 128 (2008) 105103.
[32] K.N. Hu, R. Tycko, Zero-quantum frequency-selective recoupling of homonuclear dipole–dipole interactions in solid state nuclear magnetic resonance, J. Chem. Phys. 131 (2009) 045101.
[33] A. Brinkmann, J. Schmedt auf der Günne, M.H. Levitt, Homonuclear zero-quantum recoupling in fast magic-angle spinning nuclear magnetic resonance, J. Magn. Reson. 156 (2002) 79.
[34] A. Brinkmann, M. Eden, Second order average Hamiltonian theory of symmetry-based pulse schemes in the nuclear magnetic resonance of rotating solids: application to triple-quantum dipolar recoupling, J. Chem. Phys. 120 (2004) 11726.
[35] A.E. Bennett, C.M. Rienstra, J.M. Griffiths, W.G. Zhen, P.T. Lansbury, R.G. Griffin, Homonuclear radio frequency-driven recoupling in rotating solids, J. Chem. Phys. 108 (1998) 9463.
[36] Y. Ishii, ^{13}C–^{13}C dipolar recoupling under very fast magic angle spinning in solid-state nuclear magnetic resonance: applications to distance measurements, spectral assignments, and high-throughput secondary structure determination, J. Chem. Phys. 114 (2001).
[37] A.K. Paravastu, R. Tycko, Frequency-selective homonuclear dipolar recoupling in solid state NMR, J. Chem. Phys. 124 (2006) 194303.
[38] S. Cadars, A. Lesage, N. Hedin, B.F. Chmelka, L. Emsley, Selective NMR measurements of homonuclear scalar couplings in isotopically enriched solids, J. Phys. Chem. B 110 (2006) 16982–16991.
[39] Y. Mou, J.C.C. Chan, Frequency selective polarization transfer based on multiple chemical shift precession, Chem. Phys. Lett. 419 (2006) 144.
[40] G. Pileio, S. Mamone, G. Mollica, I. Marin-Montesinos, A. Gansmüller, M. Carravetta, S.P. Brown, M.H. Levitt, Estimation of internuclear couplings in the solid-state NMR of multiple-spin systems. Selective spin echoes and off-magic-angle sample spinning, Chem. Phys. Lett. 456 (2008) 116.
[41] L. Braunschweiler, R.R. Ernst, Coherence transfer by isotropic mixing: application to proton correlation spectroscopy, J. Magn. Reson. 53 (1983) 521.
[42] B.M. Fung, A.K. Khitrin, K. Ermolaev, An improved broadband decoupling sequence for liquid crystals and solids, J. Magn. Reson. 142 (2000) 97.
[43] A.E. Bennett, C.M. Rienstra, M. Auger, K.V. Lakshmi, R.G. Griffin, Heteronuclear decoupling in rotating solids, J. Chem. Phys. 103 (1995) 6951.
[44] B.M. Fung, A.K. Khitrin, K. Ermolaev, An improved broadband decoupling sequence for liquid crystals and solids, J. Magn. Reson. 142 (2000) 97.
[45] K.V. Schenker, D. Suter, A. Pines, Broadband heteronuclear decoupling in the presence of homonuclear dipolar and quadrupolar interactions, J. Magn. Reson. 73 (1987) 99 (1969).
[46] Y. Ishii, J. Ashida, T. Terao, ^{13}C–^{1} H dipolar recoupling dynamics in^{13} C multiple-pulse solid-state NMR, Chem. Phys. Lett. 246 (1995) 439.
[47] S.-F. Liu, J.-D. Mao, K. Schmidt-Rohr, A robust technique for two-dimensional separation of undistorted chemical-shift anisotropy powder patterns in magic-angle-spinning NMR, J. Magn. Reson. 155 (2002) 15.
[48] N.M. Szeverenyi, M.J. Sullivan, G.E. Maciel, Observation of spin exchange by two-dimensional Fourier transform ^{13}C cross polarization-magic-angle spinning, J. Magn. Reson. 47 (1982) 462.
[49] A.E. Bennett, C.M. Rienstra, M. Auger, K.V. Lakshmi, R.G. Griffin, Heteronuclear decoupling in rotating solids, J. Chem. Phys. 103 (1995) 6951.